Progress In Electromagnetics Research C, Vol. 8, 107–120, 2009

EQUILATERAL TRIANGULAR MICROSTRIP ANTENNA FOR CIRCULARLY-POLARIZED SYNTHETIC APERTURE RADAR

M. Baharuddin, V. Wissan, J. T. S. Sumantyo, and H. Kuze

Microwave Remote Sensing Laboratory
Center for Environmental Remote Sensing
Chiba University
1-33 Yayoi-cho, Inage-ku, Chiba 263-8522, Japan

Abstract—An equilateral triangular microstrip antenna is proposed for circularly-polarized synthetic aperture radar (CP-SAR) systems operated in L-Band (1.27 GHz). For airborne application, a prototype antenna patch is designed, fabricated and tested. Electromagnetically-coupled, dual-feeding method is applied to generate the circularly-polarized wave radiating from the patch. The fabricated patch exhibits an axial ratio bandwidth (< 3 dB) of about 0.58% (7.4 MHz), which is consistent with the value of 0.57% (7.24 MHz) from the simulation.

1. INTRODUCTION

Synthetic aperture radar (SAR) in microwave bands is an active sensor that can produce high resolution imagery in microwave bands. The use of microwave frequencies enables penetration through clouds, and even through forest canopy for lower frequency bands. A circularly-polarized SAR (CP-SAR) to be launched onboard a micro-satellite is currently developed in the Microwave Remote Sensing Laboratory (MRSL) of the Center for Environmental Remote Sensing (CEReS), Chiba University. As part of the project, an airborne CP-SAR development is also undertaken in order to obtain sufficient knowledge of CP-SAR sensor systems. An L-band CP-SAR system will be designed for operation onboard an unmanned aerial vehicle (UAV).

Conventional SAR systems have been based on linearly polarized (LP) antenna systems. However, there are limitations due to the propagation phenomena such as the variation of geometric

Corresponding author: M. Baharuddin (merna5@graduate.chiba-u.jp).

distance between the radar system and the Earth, the occurrence of a phase shift when microwave strikes smooth, reflective surfaces, etc. These phenomena lead to unwanted modulation of backscatter signals, random redistribution of returned signal-energy and in the end, the formed image would encounter a spatially variant blurring and defocusing as well as ambiguous identification of different low-backscatter features in a scene. Especially for space propagation, electromagnetic waves propagating through the ionosphere interact with electrons and magnetic fields. As a result, the polarization vector of the electric field is rotated by the Faraday rotation effect [1]. Since the peak of ionospheric density occurs at about 400 km altitude, an L-band SAR onboard a micro-satellite orbiting at 500–800 km altitude will send and receive radar signals through most of the ionosphere.

The destructive effects mentioned above of a SAR sensor with linear polarization can be solved by the use of CP-SAR. In addition, it has been pointed out [2] that a full characterization of SAR signals backscattered from a random object can only be possible through the use of circular polarization. Hence, compared to a linear SAR sensor, a greater amount of information about scenes and targets being imaged would be provided with a CP-SAR sensor. In a study of analyzing quadrature-polarized synthetic aperture radar data from sloping terrain, Lee et al. [3] stated that the results of synthesis of circularly-polarized data are far better compared to those constructed from the conventional linearly-polarized data. In addition, more sensitive measurements can possibly be obtained using circular polarization when surface roughness is studied using polarimetric SAR data [4]. The present work focuses on the design of an L-band CP-SAR antenna. We consider the SAR system requirements to achieve an excellent performance of the overall CP-SAR system, focusing on the optimization of the single element patch.

2. CIRCULARLY-POLARIZED SAR ANTENNA REQUIREMENTS

The capability of a SAR antenna can be described by its sensitivity, spatial resolution in range and azimuth directions, image quality, ambiguities, and swath coverage [5]. Table 1 shows the specifications and targets desired for the present CP-SAR system, which in turn influence the specification of the L-Band CP-SAR antenna.

The relatively longer wavelength ($\lambda = 23.6$ cm) of L-band of 1.27 GHz ensures better penetration through vegetation canopies and snow, yielding useful information to distinguish characteristics of the earth surface. This band also provides strong returns for

Table 1. Specification of CP-SAR onboard unmanned aerial vehicle.

Parameter	**Specification**
Frequency f	1.27 GHz (L band)
Chirp bandwidth Δf	10 MHz
Polarization	Transmitter : RHCP
	Receiver : RHCP + LHCP
Gain G	>20 dBic
Axial ratio AR	<3 dB (main beam)
Antenna size	1.75 m (azimuth)
	0.5 m (range)
Beam width	8° (azimuth)
	25° (range)
Altitude range	3–10 km

larger objects and surface features [6]. The drawback associated with this choice, however, is the relatively large dimension of microstrip elements. The requirements for the range resolution (15 m) determine the antenna bandwidth of 10 MHz, or less than 1% of the operation frequency of 1.27 GHz. This bandwidth requirement must be compatible with a low axial ratio (AR) (below 3 dB) for ensuring transmitting/receiving circularly-polarized waves. To satisfy the matching of input impedance, the return loss must be smaller than 10 dB in this bandwidth range.

The primary considerations in the design and subsequent fabrication processes are low cost, light weight and ease of manufacturing. One antenna aperture will be used for both transmitting and receiving CP-SAR signals, with a circulator to control the direction of signal flow into/out from the CP-SAR sensor circuit [7]. The CP-SAR antenna consists of an array of single antenna elements, each being a microstrip antenna for circular polarization. Even though it is also possible to obtain a CP array comprising of linearly-polarized elements, the electrical performance of a CP-elements array is generally better than that of an LP-elements array [8]: Namely, (1) bandwidth of a CP-elements array is significantly wider (about twice) than that of LP-elements array; and (2) gain of a CP-elements array is significantly higher than that of LPelements array for large element spacing. The single element patches which have been optimized are then spatially arranged to form a planar array (see Fig. 1 for illustration). The planar array configuration is widely employed in radar systems where a narrow

pencil beam is needed [9]. A better control of the beam shape and position in space can be achieved by correctly arranging the elements along a rectangular grid to form a planar array. The beam pattern for optimum ground mapping function is cosecant-squared beam in the elevation plane (E-plane) which can correct the range gain variation and pencil beam in the azimuth plane (H-plane) [9]. The antenna side lobe levels in the azimuth plane must be suppressed in order to avoid the azimuth ambiguity. To deal with reflection, the antenna side lobes and back lobes also must be suppressed. The antenna gain is mostly determined by the aperture size and inter-element separation.

Feed network is implemented in a separate substrate as the feeding method is proximity coupled. The feeding array is parallel to the antenna array, corresponding to the scheme of proximity-coupled, corporate feeding. This type of feed method allows better optimization

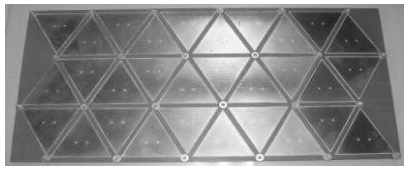

Figure 1. Configuration of a CP-SAR antenna array consisting of microstrip elements.

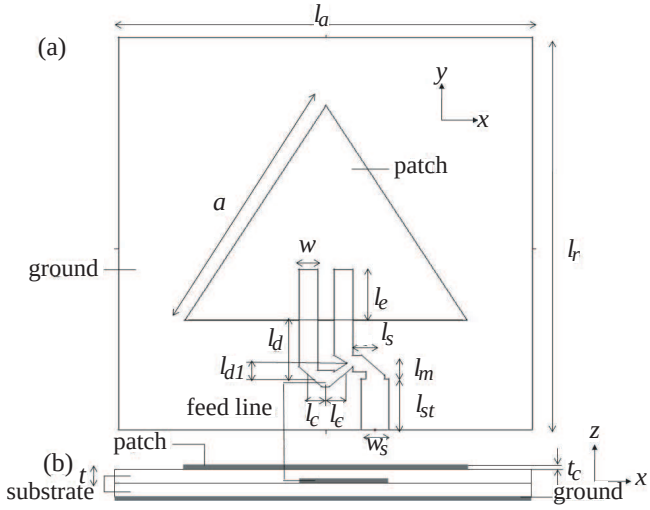

Figure 2. Configuration of equilateral triangular patch antenna with proximity coupled feed; (a) top view and (b) side view.

of both feeding and antenna array structures individually. Concept of the feed network layout proposed here is the $n \times n$ microstrip arrays with a power dividing network, consisting of an element building block of 2×2 "H" shaped feed network [10]. Constructions of a larger array can be achieved by combining the "H" networks. In the present paper, we focus on the design, fabrication, and measurement of an antenna element.

3. ANALYSIS AND DESIGN OF THE RADIATING ELEMENTS

Previously, a number of CP triangular microstrip antennas have been developed, some of them are reported in [11–13]. However, almost all the developed models implement single-feed type with coaxial probe feeding method, which possess some problems, namely: (1) the CP radiator (patch) from single feed type antenna will generate an unstable current distribution which will impair the performance of axial ratio in array configuration; (2) single feed type antenna is not preferred type for a multipolarization (RHCP and LHCP) array due to the poorer isolation parameter compared to the dual feed type one (3) according to the authors experiences, probe feed implementation is more complex in fabrication process for a CP antenna. A dual feed equilateral triangular microstrip element antenna has superior properties and would be a good element for the CP-SAR implementation.

The configuration of the radiating element together with the microstrip line feed and ground plane is shown in Fig. 2(a), where important parameters are labeled. Side view is depicted in Fig. 2(b). The equilateral triangular radiator will generate a left-handed circular polarization (LHCP) by employing the dual feed method as shown in Fig. 2(a). In order to generate a 90° phase delay on one of the two modes, the line feed on the left side is approximately $\lambda/4$ longer than the other.

Simulations with a finite ground plane model have been undertaken to optimize the size parameters using a full wave analysis tool (IE3D Zeland software) based on the method of moment (MoM) algorithm. Considering a slight difference in some geometry parameters, two types of antenna models are designed and simulated with IE3D. One is labeled Antenna-1 and another is Antenna-2. The model of Antenna-1 is designed without considering the holes for plastic screws, whereas in the design and simulation process of Antenna-2, the holes (2 mm diameter), which are reducing the area of the ground, is drawn on the ground part of the simulated model. Practically the holes are indispensable for installing the screws to assure a good coupling

Table 2. Geometry parameters (in units of mm) of the equilateral triangular patch antennas.

	Antenna-1	Antenna-2
a	102.9	102.75
w	6.9	6.8
l_d	21.5	21.5
l_e	26	27
l_{d1}	6.9	6.9
l_c	9.2	9.2
l_s	10.1	10.1
l_m	3.9	3.9
l_{st}	21.5	21.5
w_s	10.3	10.2
l_a	147.1	146.1
l_r	163.5	163.1

between the radiator and the feed line in the fabricated model. The dimensions of the radiator, microstrip feed line and the ground plane for the equilateral triangular patch are tabulated in Table 2 in units of mm. The geometry model is implemented on two substrates, each with thickness $t = 1.6\,\text{mm}$, with the conductor thickness $t_c \approx 0.035\,\text{mm}$, relative permittivity $\varepsilon_r = 2.17$ and loss $\tan\delta$ (dissipation factor) 0.0005.

During the optimization process of the microstrip line feed configuration, it was observed that the parameter l_c (distance between the two feeds) exerts a strong influence on both the CP frequency and the AR of the antenna. Fig. 3 shows the result of the simulation of Antenna-1, in which the frequency dependence of the AR is plotted for various values of the parameter l_c while keeping the other parameters unchanged. Thus, the distance must be exact in order to achieve the orthogonality of the two modes fed from the current source to the triangular patch.

The average and vector current distributions of Antenna-1 and Antenna-2 are shown in Figs. 4 and 5, respectively. From these figures, it can be observed that in Antenna-2, a significant intensity of current distribution appears in some areas outside the radiator especially near the holes, whereas in Antenna-1 those areas exhibit a much lower intensity. In addition, Fig. 5 shows that more current vectors appear in the ground area of Antenna-2, both near the radiator patch and the

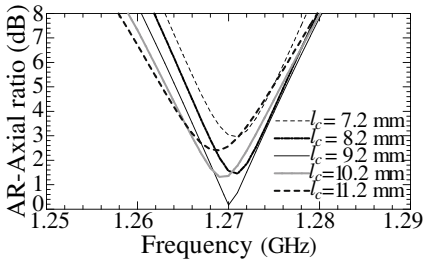

Figure 3. Simulation results showing the frequency dependence of the axial ratio (AR) of the equilateral triangular microstrip antenna for various values of l_c.

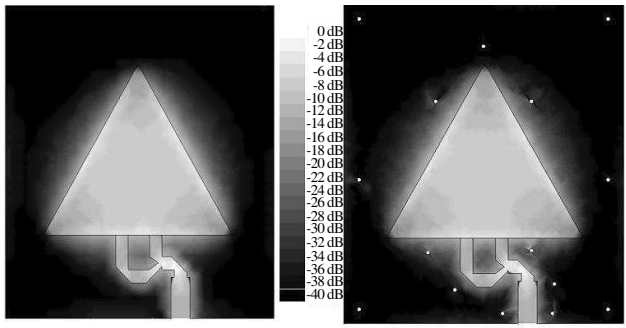

Figure 4. Average current distribution of Antenna-1 (left) and Antenna-2 (right) at 1.27 GHz.

holes near the patch. Thus, the addition of holes in Antenna-2 results in disturbing the regular vector pattern seen in the case of Antenna-1.

Even though the current distributions are slightly different for the two antenna models, the antenna efficiency from the simulation is nearly the same, 86.57% for Antenna-1 and 86.59% for Antenna-2. Also the input impedance characteristic (S_{11} parameter), gain and AR characteristics, which is a crucial parameter for circularly-polarized antenna operation, show an approximately similar characteristics (Figs. 6 and 7). In Fig. 6, input impedance bandwidth is 25.0 MHz for Antenna-1 and 26.0 MHz for Antenna-2. In Fig. 7, AR bandwidth is 7.0 MHz for Antenna-1 and 7.2 MHz for Antenna-2. Thus, Antenna-2 shows slightly better values for both input impedance and 3-dB AR bandwidth.

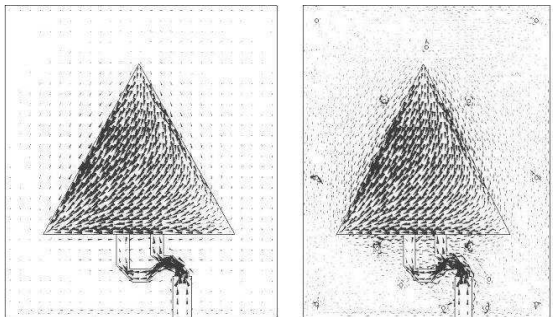

Figure 5. Vector current distribution of Antenna-1 (left) and Antenna-2 (right) at 1.27 GHz.

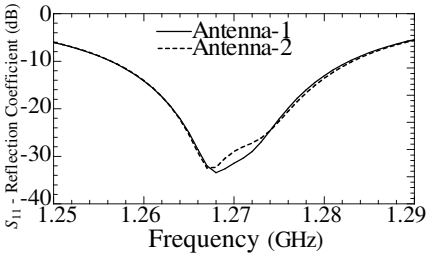

Figure 6. Simulated reflection coefficient of Antenna-1 and Antenna-2.

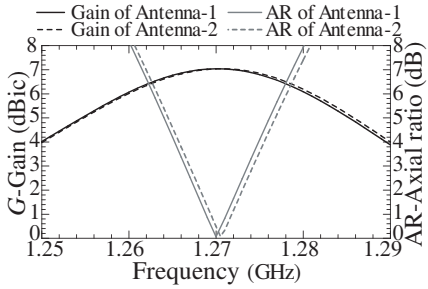

Figure 7. Simulated gain and AR of Antenna-1 and Antenna-2 at $\theta = 0°$.

4. MEASUREMENT OF ANTENNA CHARACTERISTICS

To verify the simulation results, both models (Antenna-1 and Antenna-2) with differences in some geometry parameters (Table 2) of the equilateral triangular microstrip antenna have been fabricated. From this point, the fabricated Antenna-1 and Antenna-2 are labeled Antenna-A and Antenna-B, respectively. The plastic screws are installed in the same way for both Antenna-A and Antenna-B, in accordance with the holes configuration in Antenna-2. Careful and precise fabrication process is required to produce radiating behavior similar to the simulated models. The reflection coefficient and input impedance were measured with a RF Vector Network Analyzer (Agilent, E5062A, ENA-L). The antenna gain, AR, and radiation patterns were measured inside the anechoic chamber of

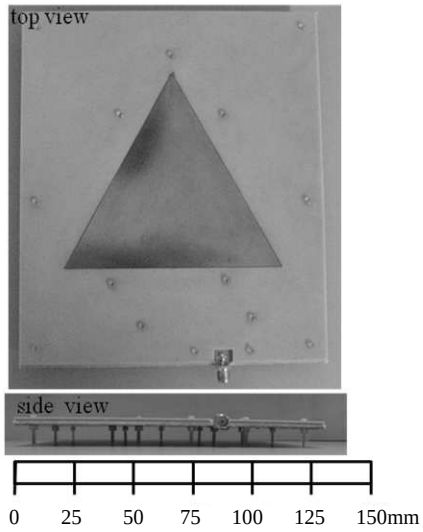

Figure 8. Fabricated equilateral triangular microstrip antenna.

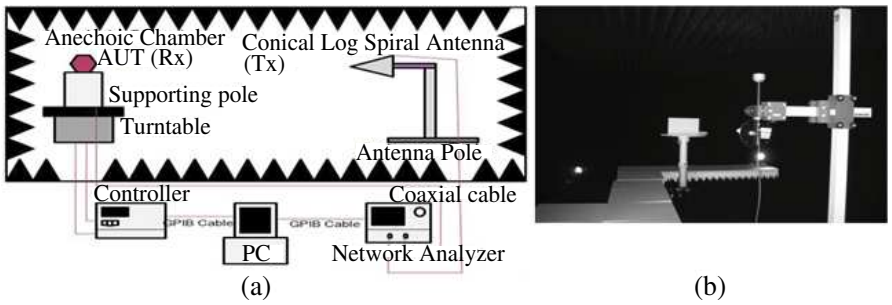

Figure 9. (a) Schematic of the measurement system. (b) Anechoic chamber at MRSL, Chiba University.

MRSL, having a dimension of $4 \times 8.5 \times 2.4\,\mathrm{m}^3$. The measurement system is schematically shown in Fig. 9 [14]. The AR vs. frequency characteristic, AR pattern, gain vs. frequency characteristic and gain pattern are measured using conical log-spiral LHCP/RHCP antennas and a dipole antenna as the standard reference. Precise alignment between Antenna Under Test (AUT) and the conical log-spiral antenna is indispensable for obtaining accurate measurement results.

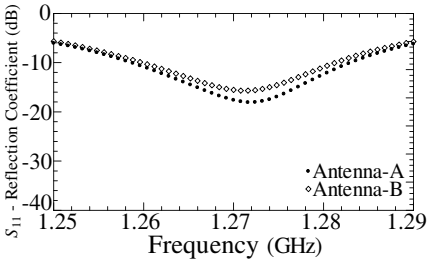

Figure 10. Measured reflection coefficient of Antenna-A and Antenna-B.

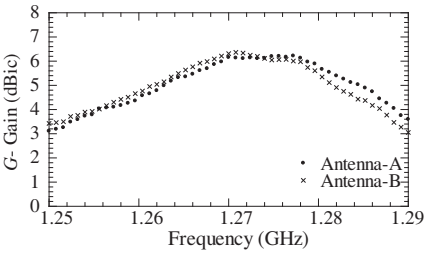

Figure 11. Measured gain and AR of Antenna-A and Antenna-B at $\theta = 0°$.

5. RESULTS AND DISCUSSION

In this part, comparison will be made between simulation results (Antenna-1 and -2) and measurement results (Antenna-A and -B) with some discussion on the comparison between the fabricated antennas (Antenna-A and -B). The experimental results are shown in Figs. 10–16. The S-parameter is shown in Fig. 10. It is found that the impedance bandwidth of Antenna-A is 24.2 MHz, which is slightly wider than the bandwidth of Antenna-B (21.5 MHz).

Figure 11 shows the gain and AR measured at $\theta = 0°$. While the gain of the antenna has been simulated to be 7.04 dBic at 1.27 GHz for both the Antenna-1 and Antenna-2 (Fig. 7), experimental results in Fig. 11 shows a smaller value by about 0.6 dB. This difference may be ascribed to the fabrication imperfections (such as inaccuracy in the milling and etching processes and connector soldering) and the substrate loss.

AR measurement results of Antenna-A and Antenna-B is shown in Fig. 12, which also shows the simulated results (Antenna-A is actually Antenna-1 with holes installed). Besides a slight difference in the center frequency, the AR characteristic of both antennas from the simulation is similar. Also from this figure it can be seen that the 3-dB AR bandwidth from the measurement is quite narrow for Antenna-A (0.1 MHz) whereas a better result of 7.4 MHz (ranging from 1.2653 GHz to 1.2727 GHz) has been obtained for Antenna-B. It can be inferred that Antenna-B retains its superior characteristics through the fabrication process and measurement condition than the counterpart. Also, it has been demonstrated that even though the size of the holes are quite small, inclusion of the effect of the holes is essential for designing a CP-SAR antenna. Even though the measurement result of 3-dB AR bandwidth of Antenna-B is slightly better than that of

the simulation result, its bandwidth is still narrower than the target specification (10 MHz). To improve this situation, the next work will consider the technique to extend the 3-dB AR bandwidth. Also the possibility to reduce the number of screws or to resort other techniques to provide a fine coupling between the feed line and the radiator patch will be explored along with the implementation of the array of antenna patches.

Figures 13–16 show the radiation pattern of Antenna-2 (simulation) and Antenna-B (measurement) in terms of gain and AR at an azimuth angle $A_z = 0°$ (and 180°, x-z plane) and 90° (and 270°, y-z) plane and at the frequency of $f = 1.27$ GHz. In Fig. 13, a difference of around 0.7 dB is seen between the simulated model and the measured antenna on the gain radiation pattern. The 5-dBic gain beam width for simulated model is 60° while the measured width is 58°. Fig. 14 shows that the simulated beam width for the 3-dB AR is 90°, while

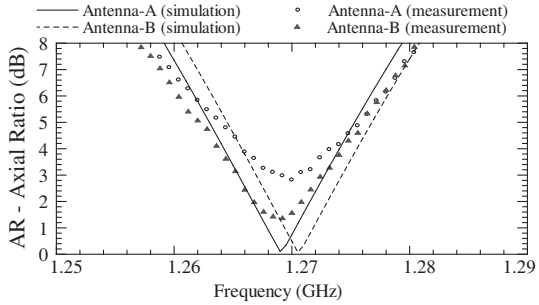

Figure 12. Simulated and measured AR of Antenna-A and Antenna-B at $\theta = 0°$.

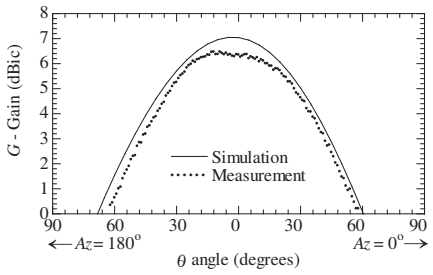

Figure 13. Gain vs. theta angle (radiation pattern) in the theta plane ($A_z = 0°$and 180°) (x-z plane) at $f = 1.27$ GHz.

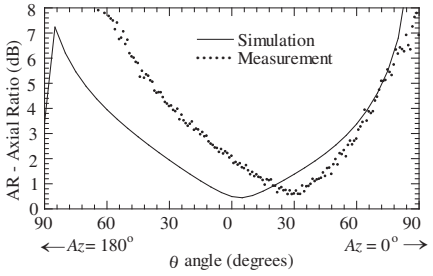

Figure 14. Axial Ratio vs. theta angle (radiation pattern) in the theta plane ($A_z = 0°$ and 180°) (x-z plane) at $f = 1.27$ GHz.

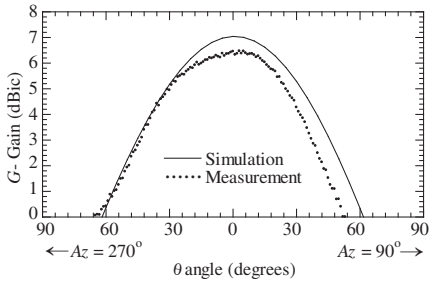

Figure 15. Gain vs. theta angle (radiation pattern) in the theta plane ($A_z = 90°$ and 270°) (y-z plane) at $f = 1.27$ GHz.

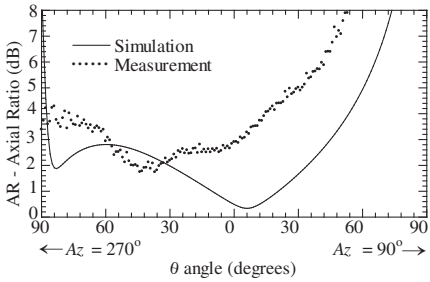

Figure 16. Axial Ratio vs. theta angle (radiation pattern) in the theta plane ($A_z = 90°$ and 270°) (y-z plane) at $f = 1.27$ GHz.

the measured width is 70°, with most beam radiated in the direction of $A_z = 0°$ ($x > 0$ in Fig. 2(a)). Fig. 15 shows the 90° azimuth measurement of gain pattern, indicating a 5-dBic gain beam width, similar to that of the 0° azimuth measurement. In this figure, beam widths are 60° and 52° for simulation and measurement result, respectively. Fig. 16 shows that the beam width simulated for 3-dB AR is 135° and the measured width is 62°, and most of the beam that has good CP characteristics is radiated in the direction of $A_z = 270°$ ($y > 0$ in Fig. 2(a)). There are some differences between the simulated and measured pattern of the antenna. This may be due to the slightly altered fabricated model and different measurement environment compared to the simulated model in the IE3D simulation environment. Especially the AR vs. angle results which show a larger difference compared with the gain one. The high sensitivity of AR behavior to the measurement condition, the infinite lateral substrate extension in IE3D, and a possible of additional radiation from the edges of the substrate in the fabricated model may contribute to the differences.

6. CONCLUSION

A circularly-polarized antenna has been developed for implementing antenna for circularly-polarized synthetic aperture radar (CP-SAR) operated in L-band. The design and optimization process was carried out using a MoM analysis software. The model was actually fabricated and measured in MRSL. Although the AR bandwidth is slightly smaller than the requirement for an airborne CP-SAR system, the present work has indicated that the goals can be met through a precise adjustment in the design and fabrication process in the near future. The slight

difference between the simulated model and the measurement results is probably due to the fabricated antenna configuration with holes for plastic nuts, connectors, etc.

ACKNOWLEDGMENT

The authors would like to thank Basari, Fauzan, Prilando R. A., Ilham A. and Zhang Jia-Yi for assisting in the antenna fabrication and measurement; the Japan Society for the Promotion of Science (JSPS) for Grant-in-Aid for Scientific Research — Young Scientist (A) (No. 19686025); Venture Business Laboratory — Chiba University for Project 10th Research Grant; National Institute of Information and Communication Technology (NICT) for International Research Collaboration Research Grant 2008, and other research grants that have supported this research.

REFERENCES

1. Rignot, J. M., "Effect of Faraday rotation on L-band interferometric and polarimetric synthetic-aperture radar data," *IEEE Trans. Geoscience and Remote Sensing*, Vol. 38, No. 1, 383–390, January 2000.
2. Raney, R. K., "Hybrid-polarity SAR architecture," *IEEE Trans. Geoscience and Remote Sensing*, Vol. 45, No. 11, 3397–3404, November 2007.
3. Lee, J., D. L. Schuler, and T. L. Ainsworth, "Polarimetric SAR data compensation for terrain azimuth slope variation," *IEEE Trans. Geoscience and Remote Sensing*, Vol. 38, No. 5, 2153–2163, September 2000.
4. Mattia, F., T. L. Toan, J. Souyris, G. D. Carolis, N. Floury, F. Posa, and G. Pasquariello, "The effect of surface roughness on multifrequency polarimetric SAR data," *IEEE Trans. Geoscience and Remote Sensing*, Vol. 35, No. 4, 954–966, 1997.
5. Pokuls, R., J. Uher, and D. M. Pozar, "Dual-frequency and dual polarization microstrip antennas for SAR applications," *IEEE Trans. on Antennas and Propagat.*, Vol. 46, No. 9, 1289–1296, 1998.
6. Birk, R., W. Camus, E. Valenti, and W. J. McCandless, "Synthetic aperture radar imaging systems," *IEEE Aerospace and Electronic Systems Magazine*, Vol. 10, No. 11, 15–23, 1995.
7. Chan, Y. K. K., B. K. Chung, and H. T. Chuah, "Transmitter and receiver design of an experimental airborne synthetic aperture

radar sensor," *Progress In Electromagnetics Research*, PIER 49, 203–218, 2004.

8. Bhattacharyya, A. K., "Comparison between arrays of rotating linearly polarized elements and circularly polarized elements," *IEEE Trans. on Antennas and Propagat.*, Vol. 56, No. 9, 2949–2954, September 2008.
9. Vetharatnam, G., C. B. Kuan, and C. H. Teik, "Microstrip antenna for airbone SAR applications," http://www.remotesensing.gov.my/images/default/publication_3rdmicrowave/3rdmicrowave_paper5.pdf.
10. Levine, E., G. Malamud, S. Shtrikman, and D. Treves, "A study of microstrip array antennas with the feed network," *IEEE Trans. on Antennas and Propagat.*, Vol. 37, No. 4, 426–434, 1989.
11. Garg, R., P. Bhartia, I. Bahl, and A. Ittipiboon, *Microstrip Antenna Design Handbook*, Artech House, Boston, 2001.
12. Suzuki, Y., N. Miyano, and T. Chiba, "Circularly polarised radiation from singly fed equilateral-triangular microstrip antenna," *Microwaves, Antennas and Propagation, IEE Proceedings H*, Vol. 134, No. 2, 194–198, April 1987.
13. Karimabadi, S. S., Y. Mohsenzadeh, A. R. Attari, and S. M. Moghadasi, "Bandwidth enhancement of single-feed circularly polarized equilateral triangular microstrip antenna," *PIERS Proceedings*, 147–150, Hangzou, China, March 24–28, 2008.
14. Wissan, V., M. Baharuddin, J. T. Sri Sumantyo, and H. Kuze, "Development of measurement system for circularly polarized synthetic aperture radar," *The 16th Remote Sensing Forum — SICE, RESTEC*, 11–12, Tokyo, March 2, 2009 (in Japanese).